1-1-2006

Lasing mechanisms in organic photonic crystal lasers with two-dimensional distributed feedback

K. Forberich

A. Gombert

S. Pereira

J. Crewett

U. Lemmer

See next page for additional authors

Lasing mechanisms in organic photonic crystal lasers with two-dimensional distributed feedback

Cite as: J. Appl. Phys. **100**, 023110 (2006); https://doi.org/10.1063/1.2210589
Submitted: 03 November 2005 . Accepted: 01 May 2006 . Published Online: 21 July 2006

K. Forberich, A. Gombert, S. Pereira, J. Crewett, U. Lemmer, M. Diem, and K. Busch

Lasing mechanisms in organic photonic crystal lasers with two-dimensional distributed feedback

K. Forberich[a] and A. Gombert
Fraunhofer Institut für Solare Energiesysteme, Heidenhofstrasse 2, 79110 Freiburg, Germany

S. Pereira
Groupe d'Etude des Semiconducteurs, Unité Mixte de Recherche du Centre National de la Recherche Scientifique 5650, Universiteé Montpellier II, 34095 Montpellier Cedex 5, France

J. Crewett
Photonics and Optoelectronics Group, Physics Department and CeNS, Ludwig-Maximilians-Universität, Amalienstrasse 54, 80799 Munich, Germany

U. Lemmer
Lichttechnisches Institut, Universität Karlsruhe (TH), 76128 Karlsruhe, Germany

M. Diem and K. Busch
Institut für Theoretische Festkörperphysik, Universität Karlsruhe (TH), 76128 Karlsruhe, Germany; Department of Physics and College of Optics & Photonics: CREOL & FPCE, University of Central Florida, Orlando, Florida 32816

(Received 3 November 2005; accepted 1 May 2006; published online 21 July 2006)

We present a detailed experimental and theoretical investigation of the lasing characteristics of organic photonic crystal lasers. These lasers are based on strongly modulated two-dimensional polymer surface relief structures on which thin films of optically active organic materials have been deposited. We determine the in-plane photonic band structure of the corresponding quasiguided modes within an effective two-dimensional model. In addition, we calculate the total (three-dimensional) losses associated with these modes. This allows us to identify the lasing thresholds for square lattice geometries and to understand the emission pattern. © *2006 American Institute of Physics*. [DOI: 10.1063/1.2210589]

I. INTRODUCTION

Photonic crystal lasers offer several unique properties compared to lasers with homogeneous gain media. In these systems, the photonic mode structure and associated dispersion relation can be tailored through several structural parameters. This facilitates an unprecedented control over the radiation dynamics of embedded active materials. In particular, low-threshold lasers may be realized and even lasers with unusual emission spectra and photon statistics have been anticipated.[1] One possibility to realize a photonic crystal laser is to use a defect as the laser cavity.[2] In this work, we concentrate on lasers where the photonic crystal provides higher-dimensional distributed feedback.[3–6] Owing to several attractive features such as broad gain spectra and easy processability, we use organic semiconductors as gain media. A particularly interesting approach lies in the combination of thin films of organic gain media with replicated plastic substrates, as this brings together two technologies suitable for low-cost, large-area production. A desirable feature of these lasers is the possibility of tuning the emission wavelength by varying the period of the underlying substrate or the thickness of the thin film of laser-active material.

In the following, we further restrict ourselves to second order lasers. In these lasers, the second diffracted order provides the necessary feedback, whereas the first diffracted order is coupled out perpendicular to the sample. Compared to first order lasers, these structures are easier to fabricate, and they also feature a built-in outcoupling mechanism. The fabrication of these devices is described in Sec. II. In order to obtain lasers with favorable properties, a detailed theoretical understanding of the linear mode structure and the lasing mechanism is required. Consequently, the general ideas of the theoretical description are laid out in Sec. III and are applied to square lattices in Sec. IV. In addition, Sec. IV features a detailed comparison between theory and experiment and a very good agreement is obtained.

II. FABRICATION OF ORGANIC PHOTONIC CRYSTAL LASERS

The microstructured substrates that provide distributed feedback were fabricated by interference lithography. In our setup, the laser beam from an Ar^+-laser operating at a wavelength of $\lambda = 363.8$ nm is split into two separate beams. These two beams are spatially filtered, expanded, and superposed on a UV-sensitive sample, typically a glass substrate coated with photoresist. In the subsequent development step, the resulting sinusoidal intensity profile is transferred into a surface relief structure. The period Λ of the structure depends only on the angle of incidence of the laser beams θ and is given by

[a]Electronic mail: karen.forberich@jku.at

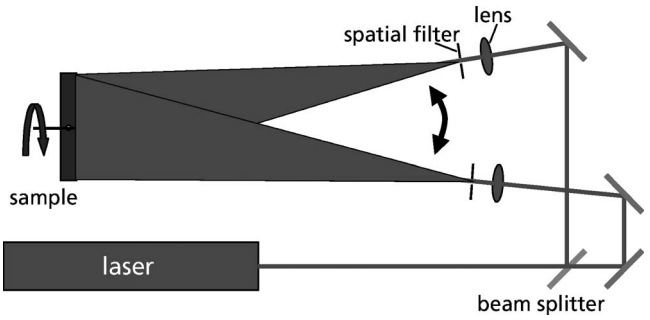

FIG. 1. Schematic of the holographic setup used for the fabrication of laser substrates. The beam of an Ar^+ laser is split into two beams which are spatially filtered, expanded, and superposed on a UV-sensitive sample. The intensity profile of the resulting interference pattern is transferred into a surface relief structure in a subsequent development step. The geometry of the resulting structure can be varied by changing the incidence angles or by rotating the sample between consecutive exposures.

$$\Lambda = \frac{\lambda}{2 \sin \theta}. \tag{1}$$

The periods that can be achieved range from $\approx 100\ \mu$m down to 200 nm. Two-dimensional patterns can be achieved by rotating the sample between two consecutive exposures. A schematic of the setup is shown in Fig. 1. The surface relief structures in photoresist can be replicated in polymers using a UV-curable lacquer, either directly or via a nickel stamp that is obtained from the photoresist through electroforming. This setup allows homogeneous structure generation on large areas for applications such as antireflective coatings or light management.[7] At Fraunhofer ISE, areas of up to 1 m^2 can be fabricated this way. Large area fabrication combined with replication leads to the possibility of low cost lasers.

The profile of the exposure dose for a structure with square symmetry which results from two subsequent exposures with 90° rotation is the sum of two sine functions. Due to nonlinearities of the development process and the photoresist, this shape is distorted during transfer into the photoresist. The exact shape depends on several process parameters such as sample preparation, resist type, exposure dose, dilution of the developers etc. It can, in principle, be determined from scanning electron micropy (SEM) and atomic force microscopy (AFM) measurements of the actual structure. A SEM micrograph of a typical structure in photoresist is displayed in Fig. 2. However, our results in Sec. IV only show a weak dependance on the exact modeling of the surface relief profile. Therefore, we neglect the nonlinearity and approximate the profile in photoresist d_{square} by the sum of two sines

$$d_{\text{square}} = \frac{d_{\text{mod}}}{4}\left[\sin\left(\frac{2\pi x}{\Lambda}\right) + \sin\left(\frac{2\pi y}{\Lambda}\right) + 2\right]. \tag{2}$$

Here, d_{mod} denotes the full modulation depth, so that d_{square} varies between zero and d_{mod}. For the active laser material, there are several possible choices such as conjugated polymers[8] or smaller organic molecules such as spirobifluorenes.[9] The measurements presented in Sec. IV were obtained using the conjugated polymer methyl-substituted ladder-type poly(para-phenylene) (MeLPPP), a very attractive π-conjugated polymer for blue light emitting diodes[10] and lasers[11] due to its high luminescence quantum yield in the solid state ($\approx 30\%$) and strong stimulated emission band[12] at $\lambda \approx 490$ nm. Our laser theory, however, makes no particular assumption about the properties of the laser material and is therefore applicable to many cases.

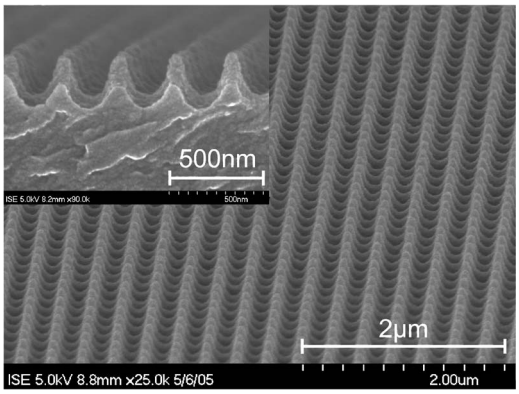

FIG. 2. SEM micrograph of a representative surface relief structure with square symmetry in photoresist. The inset shows the profile in more detail at a larger magnification.

The laser material can be applied onto the substrate either by evaporation or by spin coating, both technologies being suitable for large area and low cost production.

III. SEMICLASSICAL THEORY OF LASING

The theoretical description of lasing action from the organic photonic crystal lasers described above has to take into account the competition between the two-dimensional feedback mechanism provided by the structured substrate and the total, i.e., three-dimensional losses from material absorption and scattering. Standard distributed feedback (DFB) approaches that rely on a weakly modulated waveguiding layer cannot be applied to the present situation. Over the past years, several theoretical models relevant to lasing in periodic systems with strong modulations have been developed. However, most of them are either confined to one-dimensional (1D) or linear systems (modeling the active medium through a complex refractive index) or rely heavily on direct numerical simulations which permit only limited insight into the underlying physical processes.

Therefore, we apply the recently developed semiclassical theory of lasing action in photonic crystals[13] to the present situation of lasing from two-dimensional (2D) surface relief structures. This approach utilizes the linear eigenmodes of the structures as carrier waves and, therefore, allows us to go beyond the weakly modulated case. As a result, expressions for gain- and saturation-enhancement factors as well as the cavity losses of finite-sized systems can readily be evaluated and/or estimated from realistic mode calculations.

A. Linear eigenmodes

A planar waveguide consisting of a thin film of an organic lasermaterial on an unstructured substrate supports two

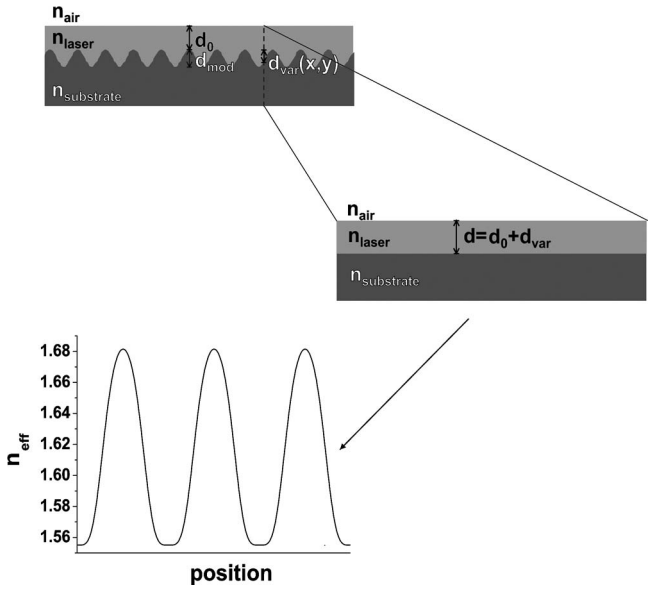

FIG. 3. Effective 2D model: at each point of the elementary cell, an effective refractive index n_{eff} is determined by calculating the dispersion relation of planar waveguide with the corresponding thickness $d=d_0+d_{\mathrm{var}}$.

types of guided modes which are characterized through their dominant electromagnetic field component perpendicular to the waveguide as either TM or TE. For a given thickness d of such an asymmetric waveguiding structure, the dispersion relation of TM and TE modes may be determined.[14] The group index at the relevant laser frequency associated with this dispersion relation then defines the effective index n_{eff} for the corresponding guided modes.

This observation allows us to analyze the surface relief structures by reducing the problem of propagation of quasiguided waveguiding modes in the plane of corrugation to an effective 2D model (Fig. 3). We achieve this mapping through translating the actual surface relief profile $d(x,y)$ into a corresponding profile of the index of refraction $n_{\mathrm{eff}}(x,y)$ for the quasiguided TM- or TE-like modes. Within this model, we consider the coupling to radiation modes into the third dimension as an additional loss associated with these modes. The spatially varying index $n_{\mathrm{eff}}(x,y)$ allows us to determine the photonic bandstructure, i.e., the linear eigenmodes, associated with TM- and TE-like guided modes. Compared to the TE-like modes, the TM-like modes exhibit a much larger overlap with the substrate, resulting in a weaker confinement and a higher laser threshold. Therefore, we subsequently concentrate on the discussion of TE-like modes.

We approximate the thickness of the polymer layer (see Fig. 3) as

$$d(x,y) = d_0 + d_{\mathrm{var}}(x,y), \tag{3}$$

where depending on the system, $d_{\mathrm{var}}=d_{\mathrm{mod}}-d_{\mathrm{square}}$ with d_{square} given by Eq. (2). In what follows, we will label the linear eigenmodes through a composite index $\alpha\equiv(n,\mathbf{k})$ that comprises the band index n and the wave vector $\mathbf{k}$. A calculated band structure for square symmetry is shown in Fig. 5.

B. Losses of the linear eigenmodes

Within the effective 2D model developed in the preceding subsection, the effective cavity loss rate γ_α associated with the linear eigenmode α consists of three independent contributions: material absorption, in-plane losses due to a finite-sized pumping region, and out-of-plane losses associated with the coupling of the (in 3D) quasiguided mode α to the radiation modes of substrate and air

$$\gamma_\alpha = 4\pi \int\int_{\mathrm{WSC}} dxdy|\mathbf{E}_\alpha(x,y)|^2\sigma_{\mathrm{eff}}(x,y) + 2(\kappa_\alpha^{\parallel} + \kappa_\alpha^{\perp}). \tag{4}$$

Here, $\sigma_{\mathrm{eff}}(x,y)$ denotes the effective material absorption within the effective 2D model that is probed by the electric field profile $\mathbf{E}_\alpha(x,y)$ of the eigenmode α within a Wigner-Seitz cell (WSC) of the photonic crystal. Furthermore, for a finite-sized pumping region, the in-plane losses $\kappa_\alpha^{\parallel}$ are identical to the rate of energy flux through the outer boundary of the pumping region. This flux is determined by the Poynting-vector $\mathbf{S}_\alpha$ associated with mode α so that ultimately the in-plane losses $\kappa_\alpha^{\parallel}$ can be estimated to be proportional to the magnitude $|\mathbf{v}_\alpha|$ of the group velocity and the local intensity I. In order to determine the out-of-plane losses $\kappa_\alpha^{\perp}$, we have computed the (three-dimensional) reflection spectra for light incident onto the surface relief grating using rigorous coupled wave analysis[15] combined with a scattering matrix technique.[16,17] This approach is only valid in the case of second order lasers and cannot straightforwardly be applied to first order lasers. The frequency dependence of the reflection exhibits peaks corresponding to the resonant coupling in and out of the quasiguided modes, i.e., the eigenmodes α in the effective 2D model. The spectral width of these peaks is a direct measure of the quality of these modes, i.e, the out-of-plane loss rate $\kappa_\alpha^{\perp}$. In order to probe different in-plane wave vectors, the light is incident under an angle θ with respect to the surface normal and its polarization is chosen so as to ensure coupling to the mode in question. The in-plane wave vector $k_{\mathrm{in\ plane}}$ can be converted into the incidence angle θ utilizing the continuity of the tangential component of the wave vector,

$$\sin\theta = \frac{k_{\mathrm{in\ plane}}}{k_0} \quad \text{with } k_0 = \frac{2\pi}{\lambda_0}, \tag{5}$$

k_0 being the vacuum wave vector and λ_0 the vacuum wavelength.

C. Lasing behavior in surface relief structures

When we combine the results of the effective 2D model with the semiclassical theory of lasing action for a two-level system with transition frequency ω_0 in photonic crystals[13] we find that the effect of the photonic structure manifests itself in a number of effective parameters that are associated with the linear eigenmodes α with electric field profile $\mathbf{E}_\alpha(x,y)$. Besides the total losses, Eq. (4), we find an effective unsaturated gain coefficient

$$\mathcal{G}_\alpha = g_\alpha \frac{4\pi|\mathbf{d}_{12}|^2\omega_0 R}{\hbar\gamma_\perp\gamma_\parallel}, \tag{6}$$

where the gain enhancement factor g_α describes how the eigenmode $\mathbf{E}_\alpha(x,y)$ with frequency $\omega_\alpha=\omega_0$ samples the effective distribution $\nu_{\text{eff}}(x,y)$ of active material within the effective 2D model

$$g_\alpha = \int_{\text{WSC}} dxdy|\mathbf{E}_\alpha(x,y)|^2\nu_{\text{eff}}(x,y). \tag{7}$$

In addition, $\gamma_\perp$ and $\gamma_\parallel$, respectively, denote the dipole dephasing and decay rate of the electric dipole moment $\mathbf{d}_{12}$ of the lasing transition. Finally, R is the incoherent pump rate at which the atoms or molecules are pumped from the lower to the upper state of the lasing transition. Likewise, we find a saturable response that may be expressed through the effective nonlinear coupling enhancement factor

$$\beta_\alpha = \frac{\int_{\text{WSC}} dxdy|\mathbf{E}_\alpha(x,y)|^4\nu_{\text{eff}}(x,y)}{\int_{\text{WSC}} dxdy|\mathbf{E}_\alpha(x,y)|^2\nu_{\text{eff}}(x,y)}. \tag{8}$$

The limiting steady-state value $I_{\text{ss}}^{(\alpha)}$ of the intensity is given by

$$I_{\text{ss}} = \frac{1}{\beta_\alpha}\left(\frac{\mathcal{G}_\alpha}{\gamma_\alpha} - 1\right), \tag{9}$$

suggesting that amplification is possible only if $\mathcal{G}_\alpha/\gamma_\alpha > 1$, and, therefore, the laser threshold condition for the linear eigenmode α is identified as $\mathcal{G}_\alpha=\gamma_\alpha$, i.e., the effective unsaturated gain compensates the effective losses. In the present case of a gain medium with a broad gain spectrum, we have to sweep the frequency ω_0 of the two-level system across the entire emission band in order to determine the overall lowest laser threshold.

In the next section, we report the results of the experimental investigations of lasing action in surface relief gratings with square symmetry and compare the experimental data with the results of the calculations based on the linear eigenmodes within the effective 2D model and their total, i.e., three-dimensional losses.

IV. RESULTS

For the measurements shown is this section, the lasers were optically pumped by a frequency doubled regeneratively amplified mode-locked Ti:sapphire laser producing femtosecond laser pulses with a temporal duration of 150 fs and a wavelength of 400 nm. The emitted light was spatially and spectrally analyzed using an optical fiber on a translation stage which was coupled to a spectrometer (Fig. 4). The structure parameters that we assumed were $n_{\text{laser}}\approx 1.7$, $n_{\text{substrate}}\approx 1.5$, a modulation depth $d_{\text{mod}}\approx 300$ nm and a layer thickness $d_0\approx 110$ nm (see Fig. 3 for the definition of the above parameters).

In Fig. 5 we display the photonic bandstructure of TE-like modes for surface relief structures with square symmetry calculated within the effective 2D model. The graph shows

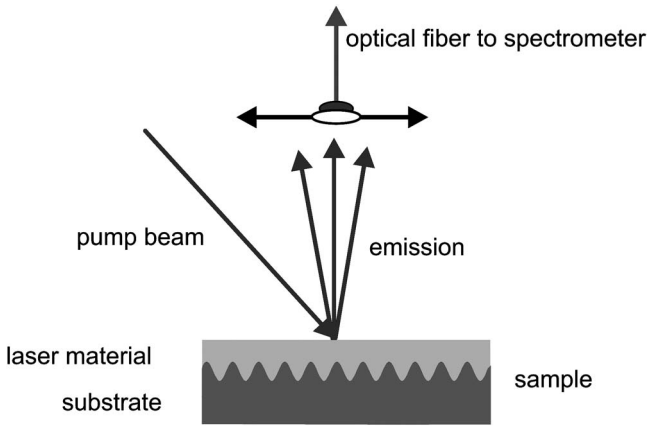

FIG. 4. Schematic of the setup for spatially resolved emission measurements. The angle-dependent emission is analyzed using an optical fiber that is mounted on a translation stage and coupled into a spectrometer.

the second to fifth band in the vicinity of the Γ point, corresponding to laser emission perpendicular to the substrate, and in Γ-X direction calculated for the above structure parameters. We notice four modes with vanishing group velocity v_g at the Γ point. To facilitate comparison with experimental data (Fig. 6), the wavelength is specified rather than energy. The experimental data shows angle-resolved photoluminescence measurements which can be identified with the bandstructure.[18] Calculations and measurements exhibit very good qualitative agreement. While the absolute values of the frequencies differ up to about 5%, the overall wave vector (angular) dependence is reproduced, the measured data showing a smaller dependance of the wavelength on the angle. The spectral resolution of the measurements is not sufficient to compare details such as the degeneracy at the Γ point. The agreement in absolute values could be further improved through a more sophisticated modeling of the surface relief profile in Eq. (2), albeit without providing further physical insight.

All the observed modes are possible candidates for las-

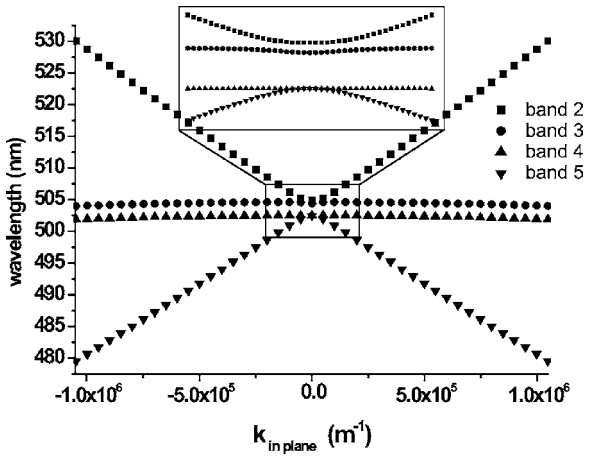

FIG. 5. Two-dimensional band structure within the effective index model for a structure with square symmetry and material parameters $n_{\text{laser}}\approx 1.7$, $n_{\text{substrate}}\approx 1.5$, a modulation depth $d_{\text{mod}}\approx 300$ nm, and a layer thickness $d_0\approx 110$ nm. Here, the second to fifth bands are shown in the vicinity of the Γ point for values of $\mathbf{k}$ corresponding to an angle of about ±5°. The inset shows the degeneracy at the Γ point.

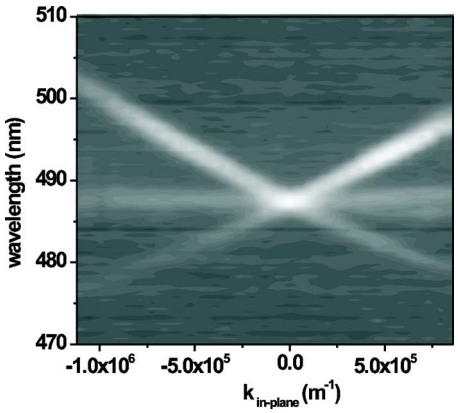

FIG. 6. Angle-resolved PL measurement for a laser based on a substrate with square symmetry. This experimentally obtained bandstructure corresponds very well to the calculated ones in Figs. 5 and 8.

ing modes as they exhibit a vanishing group velocity at the Γ point indicating low in-plane losses. The Bloch modes obtained from these bandstructure calculations were used to obtain the effective gain enhancement for all possible lasing modes. Considering the results by Florescu *et al.*[13] for structures with large refractive index contrast, we had expected to find considerable differences between the different modes. However, it turns out that these differences amount to only a few percent. Therefore, for the present weak index contrast structures the effective gain cannot be responsible for selecting the mode with the lowest lasing threshold. Instead, the out-of-plane losses largely determine the lasing threshold. Consequently, we determined the effective losses by calculating the out-of-plane losses using rigorous reflectivity calculations. In Fig. 7 we display a reflection spectrum calculated for an incidence angle of 0.3° and TE polarization of the incident light. We observe four peaks with different spectral widths. The corresponding modes can be classified as either TE-like or TM-like in the waveguide according to the magnitude of their electric field components. This classification does not necessarily agree with the polarization of the incident light.

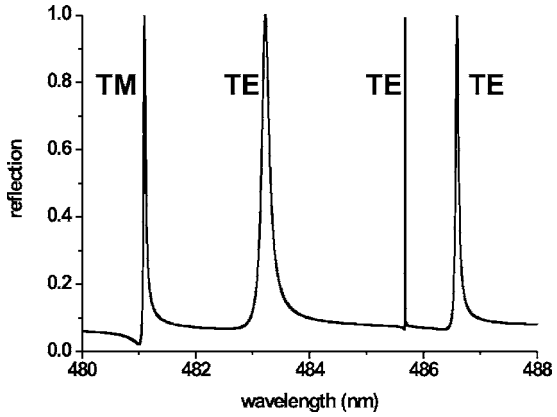

FIG. 7. Reflection spectrum calculated for an incidence angle of 0.3° and TE polarization of the incident light. We observe four peaks with different spectral widths, corresponding to different Q factors of the corresponding waveguide modes. The waveguide modes were classified as TE-like or TM-like in the waveguide according to the magnitude of their electric field components.

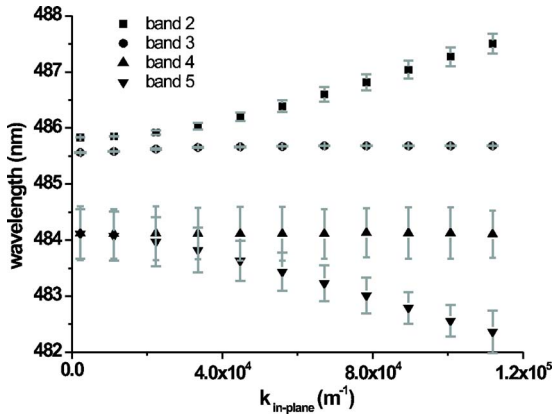

FIG. 8. Bandstructure for square symmetry determined by reflectivity calculations (d_0=150 nm, d_{mod}=210 nm). The in-plane **k** vector corresponds to incidence angles between 0° and 0.5°. The FWHM width of the observed resonances is indicated by error bars. The error bars were enlarged by a factor of 4 for visibility reasons. We observe one mode at an almost constant wavelength of $\lambda \approx 485.7$ nm, which is spectrally narrow for all incidence angles. This mode (band 3) exhibits a considerably higher Q factor than the other possible modes and is, therefore, identified as the mode with the lowest lasing threshold.

Figure 8 shows a "bandstructure" that was obtained from reflectivity calculations by determining the wavelength of the observed peaks for different angles of incidence and different polarizations of the incident light. The full width at half maximum (FWHM) width of these peaks is indicated by error bars, enlarged by a factor of 4 for better visibility. It contains only those modes that were classified as TE-like in the waveguide. The validity of this approach is supported by the fact that this bandstructure agrees qualitatively very well with the results according to the effective index model. This consistency includes the degeneracy at the Γ point. We note that for normal incidence all nondegenerate peaks vanish because of symmetry reasons. Considering the spectral width of the observed modes, we notice one mode which is about one order of magnitude narrower than all other modes (see also Fig. 7). This mode can therefore be identified as the mode with the lowest lasing threshold which can be observed in experiments. It appears on the long wavelength side of the band gap.

At pump intensities above the laser threshold, the bandstructure visible in Fig. 6 reduces to a single bright spot at the Γ point, as shown in Fig. 9. The resolution of our measurement is not high enough to verify our conclusion that the experimentally observed laser mode is to be found on the long wavelength side of the band gap. However, Turnbull *et al.*[3] have recently reported results for a very similar structure for which laser emission was found on the long wavelength side in accordance with our theoretical results.

The far-field image displayed in Fig. 10 also shows one single bright spot. At very high pump intensities, additional lines appear that can be attributed to one-dimensional feedback which is known to produce a fan-shaped emission pattern.[19] The observed laser emission at the Γ point is, at first sight, a contradiction to the fact that the narrow laser mode is a non-degenerate mode which vanishes at normal incidence due to symmetry reasons. However, this problem can be solved if we keep in mind that, differing from the

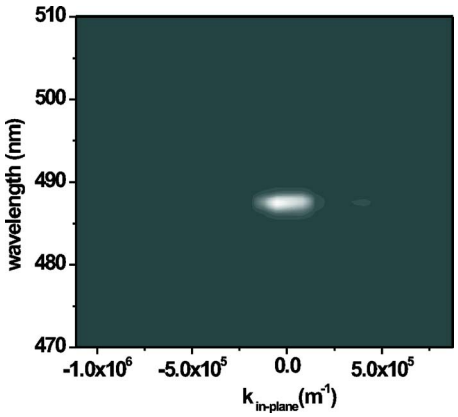

FIG. 9. Angle-resolved emission measurements for a laser with square symmetry for a pump intensity above the laser threshold. We observe one single bright spot at the Γ point, corresponding to emission normal to the surface.

assumption made in the above calculations, the real substrates are never perfectly symmetric because of instabilities in the fabrication process. In particular, the substrates used for the measurements shown above have slightly different modulation depths in x and y direction. On the other hand, the far-field pattern for a similar structure reported by Heliotis *et al.*[20] is annular which leads to the assumption that a more symmetric substrate was used in this case.

Summary

We have used a semiclassical lasing theory to describe the lasing behavior in organic, surface-emitting photonic crystal lasers with two-dimensional distributed feedback for square symmetry. The central part of our analysis has been the determination of the possible lasing modes and the calculation of the effective gain and the effective losses for each mode to identify the mode with the lowest lasing threshold. The bandstructure and the effective gain were obtained using an effective index model to project the 3D surface relief structure into the 2D plane of corrugation. The effective losses were determined by rigorous reflectivity calculations. While the effective gain is similar for all possible lasing modes, we find considerable differences in the Q factors of the different modes. The mode with the highest Q factor is therefore identfied as the mode with the lowest lasing threshold. The theoretical results are consistent with each other and also agree qualitatively well with experimental measurements, showing the validity of our approach.

With this work, it will become possible to optimize the characteristics of these and similar lasers. Specifically, a judicious design of the surface relief structure will result in a significantly lowered lasing threshold. In conjunction with optimized active materials, this may pave the way towards electrically pumped, low-cost, and large-area surface emitting lasers and laser displays.

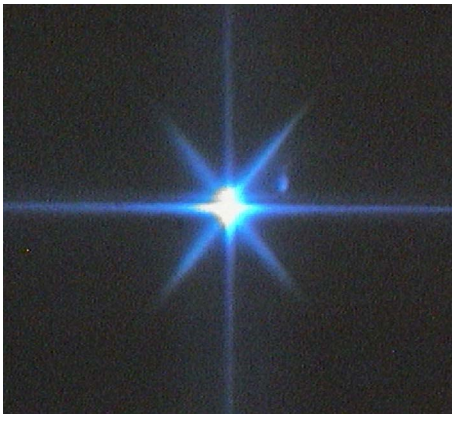

FIG. 10. Far-field pattern of the laser emission for square symmetry, from (Ref. 6). In addition to the central bright spot, several lines can be observed at very high pump intensities. These lines can be attributed to one-dimensional lasing.

ACKNOWLEDGMENTS

We acknowledge financial support by the Deutsche Forschungsgemeinschaft (DFG) within the priority program SP1113 *Photonische Kristalle* within Project No. Bu 1107/3-1, Bu 1107/3-2, Lu 204/15-1, Lu 204/15-2, Le 878/6-1, and Le 878/6-2. The research of two of the authors (M.D. and K.B.) was further supported by the DFG-Center for Functional Nanostructures (CFN) within project A 1.1.

[1] N. Vats and S. John, Phys. Rev. A **58**, 4168 (1998).
[2] O. Painter, R. K. Lee, A. Scherer, A. Yariv, J. D. O'Brian, P. D. Dapkus, and I. Kim, Science **284**, 1819 (1999).
[3] G. A. Turnbull, P. Andrew, W. L. Barnes, and I. D. W. Samuel, Phys. Rev. B **67**, 165107 (2003).
[4] M. Meier, A. Mekis, A. Dodabalapur, A. Timko, R. E. Slusher, J. D. Joannopoulos, and O. Nalamasu, Appl. Phys. Lett. **74**, 7 (1999).
[5] M. Imada, S. Noda, A. Chutinan, T. Tokuda, M. Murata, and G. Sasaki, Appl. Phys. Lett. **75**, 316 (1999).
[6] S. Riechel, C. Kallinger, U. Lemmer, J. Feldmann, A. Gombert, V. Witter, and U. Scherf, Appl. Phys. Lett. **77**, 2310 (2000).
[7] A. Gombert, B. Bläsi, C. Bühler, P. Nitz, J. Mick, W. Hossfeld, and M. Niggemann, Opt. Eng. (Bellingham) **43**, 2525 (2004).
[8] N. Tessler, G. H. Denton, and R. H. Friend, Nature (London) **382**, 695 (1996).
[9] N. Johansson, J. Salbeck, J. Bauer, F. Weissörtel, P. Bröms, A. Andersson, and W. R. Salaneck, Adv. Mater. (Weinheim, Ger.) **10**, 1136 (1998).
[10] S. Tasch, A. Niko, G. Leising, and U. Scherf, Appl. Phys. Lett. **68**, 1090 (1996).
[11] U. Scherf, S. Riechel, U. Lemmer, and R. F. Mahrt, J. Appl. Phys. **85**, 1124 (1999).
[12] A. Haugeneder, M. Neges, C. Kallinger, W. Spirkl, U. Lemmer, J. Feldmann, M. C. Amann, and U. Scherf, J. Appl. Phys. **85**, 1124 (1999).
[13] L. Florescu, K. Busch, and S. John, J. Opt. Soc. Am. B **19**, 2215 (2002).
[14] B. E. A. Saleh and M. C. Teich, *Fundamentals of Photonics* (Wiley-Interscience, New York, 1991).
[15] M. G. Moharam and T. K. Gaylord, J. Opt. Soc. Am. **71**, 811 (1981).
[16] D. M. Whittaker and I. S. Culshaw, Phys. Rev. B **60**, 2610 (1999).
[17] L. Li, J. Opt. Soc. Am. A **13**, 1024 (1996).
[18] G. A. Turnbull, P. Andrew, M. J. Jory, W. L. Barnes, and I. D. W. Samuel, Phys. Rev. B **64**, 125122 (2001).
[19] C. Kallinger *et al.*, Adv. Mater. (Weinheim, Ger.) **10**, 920 (1998).
[20] G. Heliotis, R. Xia, G. A. Turnbull, P. Andrew, W. L. Barnes, I. D. W. Samuel, and D. D. C. Bradley, Adv. Funct. Mater. **14**, 91 (2004).